Title: Investigating the effect of solubility and density gradients on local hydrodynamics and drug dissolution in the USP 4 dissolution apparatus.

Authors: Deirdre M. D'Arcy, Bo Liu, Owen I. Corrigan

PII: S0378-5173(11)00765-4
DOI: doi:10.1016/j.ijpharm.2011.07.048
Reference: IJP 12071

To appear in: *International Journal of Pharmaceutics*

Received date: 21-4-2011
Revised date: 26-7-2011
Accepted date: 30-7-2011

Please cite this article as: D'Arcy, D.M., Liu, B., Corrigan, O.I., Investigating the effect of solubility and density gradients on local hydrodynamics and drug dissolution in the USP 4 dissolution apparatus., *International Journal of Pharmaceutics* (2010), doi:10.1016/j.ijpharm.2011.07.048

*Graphical Abstract

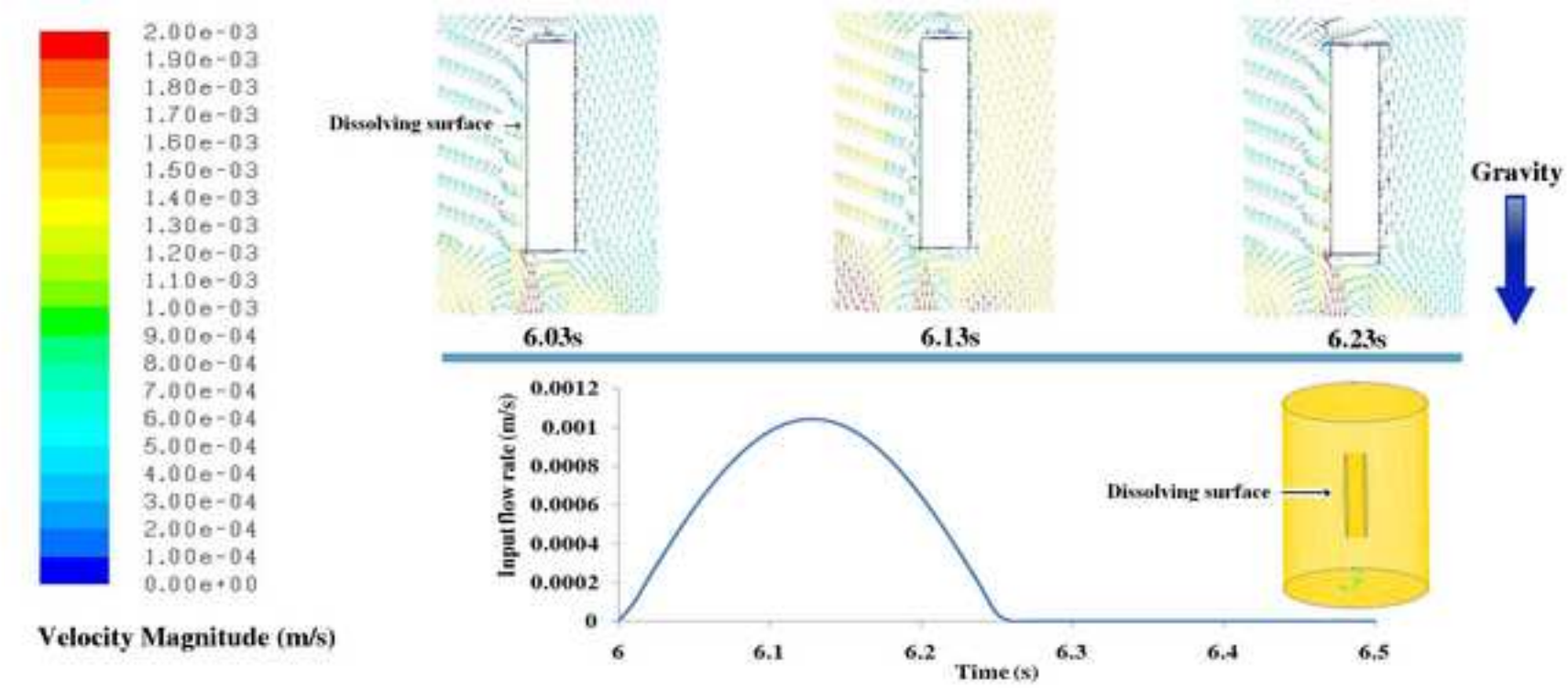

Title Page

Title:

Investigating the effect of solubility and density gradients on local hydrodynamics and drug dissolution in the USP 4 dissolution apparatus.

Authors:

Deirdre M. D'Arcy (corresponding author)

School of Pharmacy and Pharmaceutical Sciences, Trinity College Dublin,

Dublin 2, Ireland

Email: darcydm@tcd.ie

Phone: + 353 (0)1 896 2785 Fax: + 353 (0)1 896 2783

Bo Liu

School of Pharmacy and Pharmaceutical Sciences, Trinity College Dublin,

Dublin 2, Ireland

Email : liub@tcd.ie

Owen I. Corrigan

School of Pharmacy and Pharmaceutical Sciences, Trinity College Dublin,

Dublin 2, Ireland

Email : ocorrign@tcd.ie

Keywords:

computational fluid dynamics (CFD); dissolution; flow-through dissolution apparatus;

USP apparatus 4; hydrodynamics, natural convection

Investigating the effect of solubility and density gradients on local hydrodynamics and drug dissolution in the USP 4 dissolution apparatus.

Abstract

The aim of this investigation was to evaluate the effect of solubility and related solution density gradients, on hydrodynamics and dissolution rate in a low velocity pulsing flow, in the USP 4 flow-through dissolution apparatus. The paddle apparatus, flow-through apparatus and a free convection system were used in dissolution testing, using Benzoic Acid (BA) and Lactose Monohydrate (LM), representing slightly and freely soluble model compounds, respectively. A flow rate of 8 ml min^{-1} (22.6 mm diameter cell) was used in the flow-through apparatus. Computational fluid dynamics (CFD) simulations were used to analyze the effect of the dissolved compounds on local hydrodynamics. A higher dissolution rate of both BA and LM was obtained in the free convection system compared to the flow-through apparatus, with highest dissolution rate from both compounds in the paddle apparatus. The effect of downward flow arising from natural convection had a significant effect for the more soluble compound, LM, on local fluid velocities, whereas flow reversal induced by the forced convection environment was a significant feature impacting on the hydrodynamics in the BA species transfer simulation. The effect of solution density on local hydrodynamics needs to be considered when selecting dissolution conditions in the USP 4 dissolution apparatus.

1. Introduction

In vitro dissolution testing is widely used in both quality control and formulation development in the pharmaceutical industry. The flow-through apparatus (USP4) is one of the official dissolution apparatuses documented in the different pharmacopoeias (JP, 2006; Ph.Eur., 2011; USP, 2011).

The use of flow-through cells for dissolution testing of tablets and capsules was first reported in the laboratories of the United States Food and Drug Administration (FDA) over 50 years ago (Fotaki and Reppas, 2005). The flow-through apparatus was published, as an official dissolution apparatus, in the United States Pharmacopeia (USP), the European Pharmacopoeia and the Japanese Pharmacopoeia approximately 20 years ago (Fang et al., 2010). An advantage of the flow-through apparatus is that the dissolution media and flow rate can be changed during the dissolution test. Furthermore, floating dosage forms can be fixed in the center of the cell of the flow-through apparatus, which enables full contact between the dosage form and the dissolution media.

Compared to the basket and paddle apparatuses, USP apparatus 1 and 2, the flow-through apparatus can maintain theoretical sink conditions easily, especially for poorly soluble drugs, as an unlimited amount of dissolution media may be used. The effects of variation in local concentration, over the course of the pulse, on dissolution rate are likely to be more complex than a simpler picture of constant sink conditions.

Estimates of in vivo fluid velocity values vary widely, from 0.0002-0.0008 ms^{-1} from intestinal fluid transit times (Diebold, 2005), to a maximum of 0.0075 ms^{-1} from CFD simulations of a 2-D stomach (Pal et al., 2004) Although velocity spikes of up to ~0.25-0.5 ms^{-1} of a non-disintegrating tablet (particularly during the gastric emptying and colon arrival periods) has been observed, this was against a background profile of much lower tablet velocities. This illustrated both inter-patient variability and intra-patient variability over time, as measured by magnetic marker monitoring (Weitschies et al., 2010). There are notable differences in these in vivo velocity estimates, however computational fluid dynamics (CFD) simulations of hydrodynamics in the paddle apparatus predict maximum velocities relative to a compact at the centre of the base of the paddle apparatus (50 rpm) to range from 0.049 to 0.067 ms^{-1} (D'Arcy et al., 2005).

These velocities are higher than most estimates of average in vivo fluid velocity values, therefore, selection of a low flow rate in the flow-through apparatus is considered appropriate when trying to generate a bio-relevant environment. Unstable performance at flow rates at or below 6 ml min^{-1} has been noted (Fang et al., 2010). In an investigation on the development of a biorelevant dissolution method in the USP 4 flow-through apparatus, a flow rate of 8 ml min^{-1} was recommended for use in *in vitro* dissolution testing (Fang et al., 2010). The combination of the hydrodynamic environment in the flow-through apparatus with biorelevant dissolution media should be considered to create a biorelevant environment (D'Arcy et al., 2009) (Fang et al., 2010), and a flow rate of 8 ml min^{-1} in the larger 22.6 mm diameter cell combined with a biorelevant dissolution medium, was used in an *IVIVC* for a poorly soluble drug (Sunesen et al., 2005).

In terms of hydrodynamics within a flow-through system, studies investigating the effect of flow rates in different flow-through systems on dissolution rates have been widely reported ((Phillips et al., 1989; Zhang et al., 1994; Graffner et al., 1996; Butler and Bateman, 1998; Cammarn and Sakr, 2000; Bhattachar et al., 2002; Sunesen et al., 2005; Stevens and Missel, 2006; Wu and Ghaly, 2006). Furthermore, computational fluid dynamics (CFD) was recently used to simulate and analyse the hydrodynamics in the USP 4 flow-through apparatus by Kakhi (2009) and D'Arcy et al (2010) (Kakhi, 2009a; Kakhi, 2009b; D'Arcy et al., 2010).

Considering the low average velocities present in the larger 22.6 mm diameter cell, the very low Reynold's number present under flow rates of 4 to 50 ml min^{-1} (Cammarn and Sakr, 2000; Kakhi, 2009a), has previously resulted in little difference in dissolution rates observed across this flow velocity range, for a non-disintegrating system of salicylic acid dissolving in a media of pH 7.4 phosphate buffer (Cammarn and Sakr, 2000).

Hydrodynamic features present in the low velocity environment of the flow through apparatus include boundary separation at the dissolving surface, leading to flow reversal, as demonstrated

by Kakhi (Kakhi, 2009a; Kakhi, 2009b). This flow reversal affects the concentration gradient surrounding the compact surface and consequently affects the dissolution rate (D'Arcy et al., 2010).

Moreover, studies have been previously presented using numerical models which included the effect of density gradients in a very low-velocity flow-through environment, where the effect of gravity on natural convection increased with increasing solubility of solute (Stevens and Missel, 2006). It is possible to simulate the effect of the dissolution process on the local hydrodynamic environment using a species transfer model. Species transfer does not simulate the dissolution process itself, but rather is a method by which the effect of a more dense solution (the result of the dissolution process) at the surface on the surrounding hydrodynamics can be modeled. Recently, CFD results using the species transfer model have been presented, (D'Arcy et al., 2010) involving simulation of a saturated solution of the slightly soluble compound, salicylic acid, at the surface of a compact in the 12 mm diameter cell in the flow-through apparatus at 17 ml min^{-1}. The simulated results revealed that the predicted boundary layer thickness varied over the course of the pulse in the pulsing flow. Hydrodynamic simulations of the system suggested that boundary layer separation rather than natural convection was the dominant feature affecting local hydrodynamics in this system. Moreover, in the same study dissolution results of benzoic acid were presented from a lower velocity system, 8 ml min^{-1} in the 22.6 mm diameter flow-through cell, and in a system with no forced fluid flow. The results revealed that dissolution was higher in the free convection system (with no forced fluid flow) than in the flow through apparatus, suggesting a complex flow field in the flow-through apparatus at low flow rates, with low velocity pulsing flows interacting with local concentration gradients.

Although boundary layer separation was evident in the hydrodynamic simulation of flow around the compact at 8 ml min^{-1} (22.6 mm diameter cell) in the flow-through apparatus, from a simulation of hydrodynamics without species transfer, the velocities present were much lower

than at 17 ml min^{-1} in the 12 mm diameter cell (D'Arcy et al., 2010). It was suggested that at this lower flow rate natural convection may play a more significant role than at the higher flow rate of 17 ml min^{-1} (D'Arcy et al., 2010). Simulation of both species transfer and hydrodynamics within the dissolution system will give a more comprehensive prediction of both velocities and concentration gradients near the dissolving surface. Such simulations, however, are computationally expensive. There is a need to determine the effect of solubility, density and forced convection on the local hydrodynamics affecting dissolution in the low velocity environment of the flow through apparatus. This will enable prioritization of computational resources for those situations where it would be of benefit to simulate both species transfer and forced convection hydrodynamics, and those situations where it would be adequate to simulate forced convection hydrodynamics alone.

The aim of this paper was: (1) to examine the effects of different hydrodynamic regimes, influenced by both forced and natural convection effects, on dissolution of slightly and freely soluble model compounds in the dissolution apparatuses investigated; (2) to simulate, using CFD, the interacting effects of forced convection and natural convection, introduced by local density gradients, on hydrodynamics in the flow-through apparatus and a free convection system; (3) to provide an informed hypothesis as to why the dissolution rate produced in the free convection system is higher than that in the flow-through apparatus at a low flow rate.

2. Material and methods

2.1. Preparation of compacts

Benzoic acid (BA) and Lactose monohydrate (LM) were used in the dissolution studies as slightly soluble and freely soluble model compounds, respectively. Compacts used in the dissolution studies were made from 500mg BA, (VWR International Ltd., Poole, England) or LM, (Sigma-

Aldrich, Netherlands). The compacts were manufactured as previously described for BA (D'Arcy et al., 2010), where only one planar surface was exposed to dissolution media. The compacts were 13 mm in diameter and approximately 3 mm in height

2.2. Assay of samples

The concentration of BA was determined by U.V. spectrophotometry at a wavelength of 274 nm. The calibration curve was linear in the range of 0.001 to 0.1 mg mL^{-1} . The lowest concentration (0.001 mg mL^{-1}) had an average absorbance of over 10 times the highest background noise measurement, and was therefore considered to be above the limit of quantification. The LM concentrations were determined using a Lactose/D-Galactose test kit (Boehringer Mannheim / R-Biopharm, Darmstadt, Germany). The documented detection limit using the kit is 7 mg L^{-1} (Product Documentation, Boehringer Mannheim / R-Biopharm, Darmstadt, Germany).

2.3. Density, solubility and diffusion coefficient determinations.

The densities of a saturated solution of BA or LM in 0.1 M HCl (37% w/v Riedel-de Haen, Seezle, Germany) at 37°C were measured using a density bottle. The method used to measure the diffusion coefficient for LM was as illustrated in Goldberg and Higuchi (Goldberg and Higuchi, 1968), and has been described in detail for a salicylic acid/NaOH system. (D'Arcy et al., 2010). The solubility of LM in 0.1M HCl was determined by adding an excess of LM to 0.1M HCl and stirring at 37°C at 50 rpm using a magnetic stirrer, and sampling regularly until amount dissolved was no longer increasing (4 hours).

2.4. In vitro dissolution test studies

The dissolution method used for BA and LM in the flow-through apparatus and the free convection system was as previously described for BA (D'Arcy et al., 2010), with the exposed planar surface orientated vertically. 3 replicates were used in each experiment. In the flow-through apparatus the compact was held in the tablet holder. The flow through apparatus

represented a low velocity forced convection environment. Dissolution tests in a free convection system represented a static fluid condition (no forced convection) environment. Dissolution tests were carried out for BA and LM in an Erweka DT-6 paddle apparatus, in 900 ml of dissolution medium agitated at 50 rpm as previously described for BA (D'Arcy et al., 2005), representing a standard operating condition, with compacts fixed to the centre of the vessel base and the exposed planar surface was orientated horizontally. Dissolution tests were carried out in 0.1 M HCl at 37 ^{o}C, as BA would remain unionized at this pH value retaining its poorly soluble characteristics, resembling the solubility of a weak acid in the stomach in the fasted state.

Sampling times of BA in each dissolution apparatus were 15, 30, 60, 90 and 120 minutes. As disintegration was observed at later time points for LM, only the first time point was used to calculate the dissolution rate. All time points were used to determine the BA dissolution rate.

2.5. CFD simulation and construction:

2.5.1. Construction

Gambit^{TM} software (Fluent (Ansys) Inc., NH, USA) was used to build a 2-D model of the cell of the USP 4 dissolution apparatus. The flow-through cell of the USP 4 comprises two sections including a lower circular cone and an upper cylinder. During dissolution studies in the current work, the lower circular cone was filled with glass beads, with the section of hydrodynamic interest being the upper cylinder with a 30 mm height and 22.6 mm diameter. The 2-D model therefore consisted of a 22.6 mm width and 30 mm length rectangle. Two rectangles were constructed, and the smaller rectangle (representing the 2-D compact, side view) was positioned in the bigger rectangle, representing the position of the compact in the cell (2-D, side view, as shown in Figure 1 (A)). The compact in the 2-D model was based on the projection of its curved side, with the planar surface being represented in 2-D, in order to model the drug release from one planar surface of the compact.

A 2-D model of the free convection system was built as shown in Figure 1 (B). The compact in the free convection model was also the projection of its curved side.

For the 2-D models of both the flow-through apparatus and the free convection systems, lines, or virtual surfaces, were created within the geometry in order to compute the distribution of the velocity data at different positions inside the simulated models. Lines were created at different horizontal positions, at regular intervals along the compact surface as shown in Figure 1 (A and B).

2.5.2. Pump flow characteristics and hydrodynamic simulation.

The simulation of flow in the flow-through apparatus was solved in Fluent ™ (Fluent (Ansys) Inc., NH, USA). The pulsing flow was simulated using a time-dependent laminar flow model, with a time-step of 0.01s, and a half-sine-wave input flow profile generated using a user-defined function as previously described (D'Arcy et al., 2010). In each pulse, the highest velocity is at 0.12-0.13s.

2.5.3. Simulation hydrodynamics using species transfer

The species transport option (without reactions) was applied in all models in order to simulate the effect of dissolution on local hydrodynamics. Fluent can model the mixing and transport, and therefore local mass fraction, of each species by solving conservation equations of convection and diffusion for each species. (Fluent(Inc.), 2003). The specified mass fraction of solute to form a saturated solution was applied at the nodes of the boundary which represented the planar surface of the compact, simulating the effect of dissolution on fluid density adjacent to this surface. No-slip conditions were applied as boundary conditions. The diffusion coefficient was entered in the "material properties" of Fluent for either BA or LM as appropriate. A laminar model was used, and the operating conditions consisted of a fluid with viscosity of water at 37°C (6.943×10^{-4} kg

190 $m^{-1} s^{-1}$) with gravitational acceleration of 9.8 m s^{-2}. As steady state needed to be reached in the species transfer simulations, simulation over several pulses was required.

2.5.4. Velocity and concentration data for interpretation of dissolution rates and system hydrodynamics.

In the models of the flow-through apparatus and free convection systems, the velocity data on the
195 upper and lower horizontal lines (lines A and E (Figure 1 A) and lines A and C (Figure 1 B) were used to judge whether the system in the steady state. The velocity distribution present at the location of these lines was calculated over consecutive pulses, at a range of time points during each pulse. If the velocity distribution was, or was close to, overlapping at these times, it was considered that the system had come to steady state.

200 In order to investigate local and bulk hydrodynamic features of the flow through system velocity data was determined along the linear horizontal surfaces (lines A-E, Figure 1).

To determine the thickness of the diffusion boundary layer from the species transfer simulations, the concentration along the upper, central and lower horizontal lines was investigated for each model, and the "edge" of the diffusion boundary layer was defined as the point at which the
205 concentration reached 1% of the saturated solution present at the surface, as previously defined (D'Arcy et al., 2010).

2.6. Effective diffusion boundary layer thickness

The effective diffusion boundary layer thickness, h, was calculated from the dissolution data using the standard Nernst-Brunner equation assuming sink conditions:

210 $$h = \frac{C_s D}{G}$$ Equation 1

where

$$G = \frac{dw}{dt}\frac{1}{A}$$ Equation 2

$\frac{dw}{dt}$ is the change in mass with time (mg/min), C_s is the saturated solubility of the solute in the dissolution medium, D is the diffusion coefficient and A is the surface area of the dissolving surface – 1.3273 cm^2 in the current work. The assumption of sink conditions is considered valid, as the entire 500 mg compact of the poorly soluble BA dissolved in 900 ml of dissolution medium would create a solution which was 12% w/v of the saturated solution concentration. In the current work, in no case was the entire compact dissolved.

3. Results and Discussion

3.1. Density and diffusion coefficient in 0.1 M HCl.

The densities of the saturated BA and the saturated LM solutions were 997.2+/-0.2 g L^{-1} and 1091.1+/-0.9 g L^{-1} respectively. By contrast, the density of the dissolution medium, 0.1M HCl, was 995.3 g L^{-1}. The diffusion coefficient of LM was measured as 3.19 x 10^{-10} m^2 s^{-1}. The experimentally determined result for the diffusion coefficient of LM is comparable to the reported value 5-5.5x 10^{-10} m^2 s^{-1} , for LM in water at 30°C (Venancio and Teixeira, 1997). The solubility of LM in 0.1M HCl was 219.64 g L^{-1}. The solubility of BA was taken to be 4.564 g L^{-1} (Ramtoola and Corrigan, 1987) and the value used for the diffusion coefficient of BA was 1.236 x 10^{-9} m^2 s^{-1} (Edwards, 1951).

3.2Dissolution profile and dissolution rate

The dissolution results are shown in Table 1. The dissolution rate of BA was highest in the paddle apparatus, at 3.6 times that in the free convection system and 4.7 times that in the flow-through apparatus. The dissolution of BA was shown previously to be notably faster in the free convection

system than in the flow-through apparatus (D'Arcy et al., 2010). In the current work, the calculated parameter for h (equation 1) illustrates that the effective diffusion boundary layer is thinner in the free convection system than in the flow through apparatus. As the effective diffusion boundary layer is proportional to the hydrodynamic boundary layer, these results suggest that the hydrodynamics in the vicinity of the dissolving surface are different in each apparatus. The thinner effective diffusion boundary layer within the same dissolution system (apparatus and geometry) is associated overall with higher local velocity values. The stronger agitation in the paddle apparatus contributed to the dissolution rate of BA in the paddle apparatus being highest overall, with the smallest estimate for h in this system for BA. The dissolution rate of LM was also fastest in the paddle apparatus, with the smallest overall h for any system being estimated for LM in the paddle apparatus. Similarly, the dissolution results for LM demonstrate that the effective diffusion boundary layer was thinner, and therefore dissolution faster, in the free convection system than the flow through apparatus. The difference between the estimated h values for LM in the free convection system and the paddle apparatus is much less than that for BA, illustrating the combined effect of compact orientation and solution density, as the dissolving surface was vertical in the flow-through apparatus and horizontal in the paddle apparatus. Although the agitation conditions were stronger in the paddle apparatus, natural convection could play a greater part in the free convection system where the vertical surface facilitated downward flow of the more dense saturated solution. It is interesting to compare the effective diffusion boundary layer estimates for LM and BA. Despite being in the same dissolution apparatus at the same flow rate, the estimated h for LM is approximately 2.8 and 4.5 times less than BA in the flow-through apparatus and free convection systems respectively. These results imply that the process of LM dissolution can have a significant effect on the local hydrodynamics, in both the free convection system and in the low-velocity pulsed flow of the flow-through apparatus. This observation, together with the fact that for both the slightly soluble BA and freely soluble LM, the dissolution rate in the free convection system was higher than in the flow-through apparatus,

indicate that there is a complex interaction between local hydrodynamics and natural convection in the dissolution apparatuses investigated. The local hydrodynamic environment generated by each combination of dissolution system and solute will be discussed in detail in the next section.

3.3. Simulated hydrodynamic and species transfer results

3.3.1 Initial and steady state in the systems modeled.

In the current work, simulations are presented from the initial state and steady state. The initial state is given by the simulation of the first pulse, where it is considered that species transfer will not have had the opportunity to significantly affect the local hydrodynamics.

As described in section 2.5.4, the velocity distribution present at the location of a series of lines extending horizontally from the compact surface was calculated over consecutive pulses, at a range of time points during each pulse. When the velocity distribution was overlapping at these time points for two consecutive pulses, it was considered that the system had come to steady state.

The model simulating species transfer of BA in the flow through apparatus reached steady state during the 9^{th} pulse commencing at 4.01 s, and that of LM during the 13^{th} pulse commencing at 6.01s.

In the free convection system, steady state was reached after 8.5 seconds for the simulation of BA species transfer, and after 6.5 seconds for the simulation of LM species transfer.

3.3.2 Hydrodynamic simulations including BA species transfer in the flow-through apparatus and free convection system

CFD generated vectors of velocity magnitude in the flow-through apparatus, incorporating the simulation of BA species transfer, demonstrated an obvious hydrodynamic flow reversal adjacent

to the compact surface, in both the initial (first pulse) and steady states, as shown in Figure 2 (C and F). Previously presented CFD simulations of a 3D model without species transfer demonstrated that flow reversal had already occurred during the zero inflow period of the first pulse (0.35s) (D'Arcy et al., 2010). In the current work, comparing the flow vector profiles of the BA species transfer model in the flow-through apparatus at the initial state and steady states, the separation of flow happened at the same time point in each case, at approximately 0.23s in each pulse. This indicates that the timing of flow separation is not affected by the species transfer. Rather, the adverse pressure gradient played the primary role in causing flow reversal, as described previously by Kakhi (Kakhi, 2009b). The downward flow direction (flow reversal) following boundary separation is opposite to the bulk flow direction and counteracts the upward bulk flow induced by forced convection.

The fluid velocity distribution at both the initial and steady state in the region surrounding the compact boundary is illustrated using vectors coloured by velocity magnitude in Figure 2. Although the solubility and density of BA solution is not as high as that of the LM solution, there was a slight effect on the local hydrodynamics. This was manifest as a slight increase in the flow reversal at 4.23s (Figure 2F) and a marginal reduction in the surrounding flow at 4.13s (Figure 2E, maximum inflow) when the system was at steady state, in comparison to the corresponding time points in the initial state, Figures 2C and 2B respectively.

A more detailed quantitative analysis of the velocity magnitude distributed on horizontal lines A to E (described in Figure 1) in the flow-through apparatus, is shown in the Figure 3. The velocity magnitude distribution on each line was compared at 0.13s (Figure 3A, maximum inflow, initial state) and 4.13s (Figure 3B, maximum inflow, steady state). In terms of the bulk flow field (approximately 2-8 mm from the compact surface), the velocity magnitude distribution was similar on line A to E at 0.13s and 4.13s, with a maximum velocity of approximately 0.0012 to 0.0014 m s^{-1} at a distance of 2-8 mm from the compact surface, with a slightly increased velocity

at 4.13 s. The overall picture therefore suggests that the relatively slow dissolution of BA does not influence the bulk region of the flow field. Therefore, a drug, with low solubility and similar saturated solution density as BA dissolving in 0.1 M HCl in the flow-through apparatus, will not significantly affect the bulk fluid flow in the flow-through apparatus.

In contrast, the quantitative analysis of the flow in the region of 0 to 2 mm from the compact surface reveals a minor change in flow velocity near the compact surface. There was a notable decrease in the velocity distribution curve in this region, as illustrated in Fig 4A and Fig 4B, between the initial and steady state. The difference in fluid velocity between the initial and steady state is most evident on lines A and E, which were near the top and bottom of the compact, respectively. The velocity profiles on these lines differ to those on lines B, C, and D in both the initial and steady state due to the more complex flow arising from edge effects near the top and bottom of the vertical compact surface. There is a decrease in velocity magnitude evident in this region near the compact surface on lines B, C, and D also (Figure 3 (A) versus (B)). The decrease in the flow velocity near the compact surface may be caused by gravitational effects on the more dense saturated solution of BA at the surface, slowing the upward forced convection at this point of maximal inflow of the pulsing flow. On the other hand, it is possible that there are some changes in local flow between the pulses at the initial and steady state independent of any natural convection effects, as each pulse at steady state will be affected by residual motion from the previous pulse, a condition not present in the initial state. Therefore, in order to investigate the nature of the flow direction and magnitude which can be induced by gravitational forces acting on the more dense bulk solution, a free convection system was simulated.

The velocity vectors in the free convection system generated by CFD are shown in the Figure 4. The diffusion of BA into the bulk flow field in the free convection system extended very slowly due to a low overall species transfer rate. Despite the low species transfer rate, the more dense BA solution induced a consistent downward flow near the dissolving surface due to natural

convection. As there is no other force affecting or countering the flow direction or magnitude in the free convection system (unlike the opposing flows in the flow-through apparatus) the unobstructed downward flow of the BA solution formed, maintaining the concentration gradient at the dissolving surface, may explain the increased dissolution rate of BA in the free convection system compared to the flow-through apparatus (Table 1).

In the free convection system, the highest velocity was below the surface of the BA compact exposed to the dissolution media, since the surface is a constant source of species. The BA will move from the saturated solution at the compact surface to the bulk dissolution media along a concentration gradient. However, as the saturated solution is more dense than the bulk medium, and the compact is fixed to the top of the free convection system, downward flow is also introduced along a density gradient under the influence of gravity. In terms of velocities generated at the dissolving surface, the maximum velocity increased to approximately 1.3×10^{-4} m s^{-1}, near the upper edge of the compact. Although a velocity stream was generated due to natural convection, this is still a very low overall velocity, as illustrated in Figure 4A. This was much lower than the bulk mainstream velocity in the simulation of the flow-through apparatus with BA species transfer of approximately 1.4×10^{-3} m s^{-1}, as shown in Figure 3. These low velocity values generated in the free convection simulation suggests that the low velocity region produced by the BA dissolved in the free convection system could have, at most, a minor effect on the flow velocities near the dissolving surface in the flow-through apparatus at 8 ml min^{-1}. It is unlikely that gravitational effects on the more dense BA solution could overcome the upward flow, or completely reverse the flow, under the conditions simulated in the flow-through apparatus. The flow velocities in the flow-through apparatus under the conditions investigated during the dissolution of the BA compacts were predominantly controlled by forced convection and associated effects such as boundary layer separation and flow reversal. During the low- or zero-velocity periods of the pulse in the flow-through apparatus, the simulations of the free convection

system demonstrate that gravitational effects may have been able to influence local hydrodynamics, though flow reversal had already occurred at this point following hydrodynamic boundary layer separation.

Although the BA solution will not alter the hydrodynamics in the flow-through apparatus to the same extent as the more dense LM solution (section 3.3.3), it is possible that the denser BA solution (relative to the dissolution medium) increased the downward flow that was initially caused by flow reversal. The decrease in flow in the region close to the compact surface due to the boundary separation and/or flow reversal, with the effect enhanced by gravitational effects on the denser BA solution, affected the movement of BA from the surface to the bulk. The dynamic alteration between weak upward and downward flow near the dissolving surface will affect the effective diffusion boundary layer thickness and therefore the concentration gradient driving dissolution. As the flow slows and changes direction the boundary layer will increase, while flow reversal will increase the amount of solute present near the dissolving surface. Both of these effects will serve to inhibit dissolution in the flow-through apparatus.

In order to examine the effect of flow on the boundary layer, its thickness was examined over the course of the pulse, on the upper, central and lower horizontal lines. The boundary layer thicknesses on the line extending horizontally from the centre of the compact surface in both the flow-through apparatus and free convection system, are shown in Figure 5. The boundary layer was "thicker" at all time points at the lower edge of the compact than the upper edge (not shown). The boundary layer thickness on the central line, of approximately 4.5×10^{-4}m, was similar to that on the lower line. In contrast, in the free convection system, there was no change in boundary layer thickness between the lower, central and upper lines. The boundary layer thickness on the central line in the free convection system was approximately 4.3×10^{-4} m (Figure 5), and is less than that determined for the flow-through apparatus on the central line, at all time points over the pulse. Although the difference is small, the fact that the boundary layer is consistently thinner in

the free-convection system than the flow-through apparatus is consistent with the higher dissolution rate for BA observed in the free convection system. Thus, the local hydrodynamics in the flow-through apparatus at this flow rate result in a system generating a lower dissolution rate, from a vertical surface of a compound with a solubility and density of BA in 0.1M HCl, than the dissolution rate observed in the free convection system.

In a previous simulation of species transfer from a salicylic acid compact in the 12 mm cell at 17 ml min^{-1}, it was observed that the predicted diffusion boundary layer thickness was thicker at the upper end of the compact than the lower end (D'Arcy et al., 2010). This previous simulation was of a system with a higher overall velocity than that used in the current work, consequently there were very strong fluid recirculation zones, near the top side of the compact, which resulted in a lesser concentration gradient and thicker boundary layer in this region. In contrast, in the current work, which is a lower velocity system, the diffusion boundary layer thickness in the flow-through apparatus is thicker at the lower end of the compact than the upper end. The contrast between these results illustrate that not only overall velocity magnitudes, including those due to natural convection, are relevant, but also any hydrodynamic features such as eddies and recirculation zones should be considered in terms of the effect on local concentration gradients.

3.3.3 Hydrodynamics simulations including LM species transfer in the flow-through apparatus and free convection system.

The density of saturated LM solution is considerably higher than that of dissolution media (section 3.1). The ratio of the density difference ($\Delta\rho$, where ρ is density) between the saturated solution and bulk solution for LM and BA can be given as $\Delta\rho$LM: $\Delta\rho$BA. From the experimental data, this ratio was calculated to be approximately 50, which illustrates the more significant density gradient generated by the LM solution, enabling it to produce a stronger and more

powerful downward flow based on gravity than the BA solution. Although flow reversal adjacent to the compact surface could be observed at 0.23s in the initial state (Figure 6 C), similar to that observed in the BA simulation (Figure 2C), the flow pattern near the surface at steady state (6.23s, Figure 6 F) was quite different from the initial state. Downward flow was observed at different time points across the pulse including 6.03, 6.13 and 6.23s at steady state (Figure 6 D-F), indicating that the downward flow of more dense LM solution was the dominant force near the surface of the dissolving LM compact. However, the upward bulk flow cannot be entirely neglected, as this counter-flow can reduce the dissolution rate of LM compared to that in the free convection system.

Quantitative analysis of velocity magnitude distribution during LM species transfer in the flow-through system at the initial state was consistent with the flow rate being initially controlled by forced convection, since velocity magnitude distribution of the models simulating BA species transfer and LM species transfer at initial state were similar, in Figure 2 A-C and Figure 6 A-C. When the species transfer of LM was at steady state (Figure 6 D-F), the region influenced by the LM dissolution process was significantly larger than that in the BA dissolution system, affecting a region up to 4 mm away from the compact surface. In this region, the velocity was complex, as shown in Figure 7, which is taken from the simulation at maximum inflow velocity, at 6.13 s. Figure 7 shows that after the initial velocity increase moving away from the compact surface, there was a decrease to almost zero velocity at a position around 1 mm from the compact surface. This suggests that the downward flow produced by the LM species transfer may counteract the upward flow produced by the forced convection by an approximately equal force at this point, even at the point of maximum inflow velocity. This 1 mm position away from the tablet surface can be labelled as a transit point. From the surface of the compact to the transit point, the natural convection produced by the LM species transfer was dominant, with the highest velocity around 0.0017 m s^{-1}. In contrast, from the transit point to the wall of the flow-through cell, the flow

produced by the forced convection was dominant, with the velocity reaching 0.0013 m s^{-1} to 0.0017 m s^{-1} (Figure 7) The velocity distributed on line E was different to the velocity distribution on the other lines, with only a slight increase and decrease in velocity near the compact surface. The flow then increased to the velocity of the bulk flow region, which was established at a point nearer the compact surface in the region of this upper line than was apparent on the lower lines A-D. As Line E is close to the upper edge of the compact, there is little accumulation of LM solution at this position, due to the overall downward flow of LM. Compared to other positions on the compact surface, the effect from the density gradient was much smaller near this upper edge. The main force dominating the flow distribution profile at the position of line E, at the time points illustrated, was therefore forced convection, which is further compounded by the inward flow over the upper edge of the compact at this location (Figure 6).

The velocity vectors of the LM species transfer in the free convection system generated by the CFD are shown in Figure 4B. The LM dissolution rate was significantly higher than that of BA in the free convection system due to a higher density of saturated LM solution as well as a higher solubility of LM, as reflected in the h values presented in Table 1. When the LM species transfer simulation was at steady state, the region of the free convection system affected by LM species transfer (Figure 4B) was notably larger than that of the BA species transfer (Figure 4A).

The simulated maximum velocity in the free convection system when it reached steady state, was approximately 0.002 m s^{-1} near the lower edge of the compact. Comparing this velocity value to velocities present in the flow through apparatus (maximum ~0.0017 m s^{-1}, Figure 7), suggests that when LM dissolved in the flow-through apparatus, the natural convection produced by the LM dissolution could alter the hydrodynamics in the cell of the flow-through apparatus at 8 ml min^{-1}.

Contrary to the situation in the BA species transfer model of the flow through apparatus, the species transfer of LM was partly driven by the flow generated by the LM solution itself as it

dissolved. This flow was countered by the upward forced convection, reducing the potential for downward flow from the LM solution. The effect from the upward forced convection is a dynamic one, as the forced convection magnitude, and therefore the potential effect of natural convection on forced convection, changes over the course of the pulse. This repeated slowing, by upward forced convection, of the downward flow produced by the forming LM solution will affect the local concentration gradient, as the effective diffusion boundary layer broadens in a lower velocity field. The effect on concentration gradient is similar to that observed in the BA dissolution system, except that in that case the flow governing dissolution is the forced convection, with both boundary layer separation and local density gradients slowing the upward forced convection.

The diffusion boundary layer thickness on the central horizontal lines (Figure 5), revealed a thicker diffusion boundary layer in the flow-through apparatus (~2 x 10^{-4}m) than in the free convection system (~1.1 x 10^{-4}m), consistent with the lower dissolution rate in the flow apparatus compared to the free convection system. It is worth noting that this central boundary layer thickness between the upper and lower lines in the flow-through apparatus was thinner than that in the BA species transfer model in the flow-through apparatus.

The difference between calculated boundary layer thickness on the lower and upper lines was greater in the free convection system than in the flow through apparatus (1.1 x 10^{-4} m (upper) versus ~2.2 x 10^{-4} m (lower) in the free convection system, and 1.1-1.5 x 10^{-4} (upper) versus ~2 x 10^{-4} m (lower) in the flow through apparatus). The upper line in the flow through apparatus may have been affected by recirculation zones in the bulk flow generated by the flow reversal at the surface (Figure 6 D-F), resulting in a thinner diffusion boundary layer in this region.

The boundary layer thicknesses on the central lines do not change over the course of the pulse as shown in Figure 5. The thickness was noted to change along the lower line in the model

simulating BA species transfer and the upper line in the LM species transfer model. In the BA species transfer model, the boundary layer thickness increased during the second half of the pulse, consistent with the decrease in forced convection during this period. In the LM species transfer model, however, the boundary layer thickness on the upper line was reduced during the second half of the pulse. This can be attributed to a reduction in the upward forced convection, and therefore a reduction in the counterflow to the downward flowing natural convection. The constant boundary layer thickness over the course of the pulse on the central lines depicted in Figure 5 may be due to the arbitrary definition of the "edge" of the boundary layer at the point where the concentration was less than 1% of the saturated concentration. On examination of the mass fraction of BA over the course of the pulse at varying distances from the compact surface, the concentration along this central line was noted to change over the course of the pulse. With the LM simulation, the concentration increased at the point where the forced convection increased, consistent with the observation that the counterflow of the forced convection decreased the natural convection induced by LM (Figure 6). With the BA simulation, the mass fraction along the central line was noted to continuously increase. This may be due to the continuous source of BA in the system, causing the concentration to increase overall before reaching an equilibrium with outflow. However it may also reflect the local buildup of BA at each location during the later part of the pulse when the forced convection had reduced.

In each case, in the free convection system once a natural convective flow is established, there is no forced convection flow countering it to interfere with the local concentration gradient. Thus, with the velocities and solubilities investigated in the current work, the dissolution rates in the free convection system for both LM and BA were higher than in the flow-through apparatus. This observation is supported by the predicted differences in diffusion boundary layer thickness, and therefore concentration gradient driving dissolution, in particular in the central region of the compact, between the free convection and flow-through dissolution systems. Furthermore,

particularly in the case of the more dense lactose solution, a density gradient develops within the flow-through cell over time, as the more dense solution is present towards the bottom of the cell. This would naturally be disrupted with each new pulse, however, overall it is possible that the effluent concentration might be less than the average concentration at the base of the cell. Nevertheless, over the course of the dissolution, an equilibrium should be established allowing quantitative comparison of dissolution results from effluent concentration. The timescale required for such an equilibrium to develop is beyond the scope of the current simulations.

The current work simulates how a saturated solution at the dissolving surface could affect local hydrodynamics via gravitational effects on density gradients. As the velocity and therefore concentration gradients change over the course of the pulse, issues of the effective available volume require consideration. This is of particular interest as in the case where the flow slows and changes direction, the effective volume available to drive the dissolution process via the concentration gradient is dynamic in nature. The effects of volume available on dissolution rate in terms of the relevance and use of reaction-rate limited dissolution models has been recently presented (Dokoumetzidis et al., 2008). However, this theory would need to be extended to consider the use of such models at certain time points in a dynamic, changing flow system, such as the pulsing flow of the flow-through apparatus, in order to be applied to the situation outlined in the current work. Furthermore, the current study considered a static dissolving surface in a low velocity pulsing flow. The effect of natural convection on local hydrodynamics for mobile particulate system is a separate scenario, as the particles will be subject to different local relative velocities depending on their density and size (D'Arcy and Persoons, 2011).

The current work used CFD to simulate hydrodynamics and velocity magnitudes within the flow-through apparatus dissolution cell. A recent study considering hydrodynamics in the 22.6 mm diameter cell used magnetic resonance imaging (MRI) as a method to determine the local fluid velocity magnitudes and overall hydrodynamic patterns in the flow-through apparatus (Shiko et

al., 2010). Dynamic flow movement was observed by MRI at a range of flow rates in both the 12 mm and 22.6 mm diameter cells. Although the compact dimension, orientation and location was different to that in the current work, the velocities observed were overall low, with notable variation across the cell. In particular, flow reversal was observed near the cell wall. The results also indicated that a change in tablet orientation in the flow-through apparatus would lead to a significant variation in flow velocity. The results presented in the current work can be interpreted with relevance to a compact positioned vertically at the centre of the cell. Furthermore, it can be concluded that the low and variable velocities present over the course of the pulse in the cell allow a potentially significant contribution from natural convection, depending on the solubility and position of the dissolving surface.

Evidence is growing that lower agitation rates, resulting in lower fluid velocities, as provided by the USP 4 dissolution apparatus can be considered more biorelevant (D'Arcy et al., 2009)(Sunesen et al., 2005; Fang et al., 2010). Thus the results presented in the current work impact on the selection of biorelevant dissolution test conditions. The extent to which density gradients influence dissolution *in vivo*, is difficult to predict. However, given that fluid velocities are considered to be inconstant, with periods of low velocity overall, it is likely that local density gradients will influence the drug dissolution rate. For example, the presence of soluble excipients in a formulation should cause increased localized natural convection in the vicinity of the drug, reducing the effective aqueous boundary layer thickness and thus enhancing drug dissolution, the effect becoming more dominant the lower the overall agitation conditions. In addition, at the early formulation development stage, using large proportions of excipients with differing solubilities may lead to different dissolution rates under the same low velocity conditions. As a result, it can be concluded that along with selecting biorelevant media, the effect of natural convection generated by the dissolving surface is relevant when attempting to determine the appropriate fluid velocity environment to construct an *IVIVC*

4. Conclusion

Both flow reversal following boundary separation and species transfer affect the local hydrodynamics and therefore the dissolution rate at 8 ml min^{-1} in the flow-through apparatus under the conditions investigated. For a freely soluble compound, such as LM, the denser flow could overcome upward inlet forced convection, with a downward counter-flow predicted over the course of the whole pulse at steady state. The notable effect of the species transfer from LM on the system hydrodynamics implies that simulation of both species transfer and hydrodynamics is necessary to interpret dissolution rates of a freely soluble compound under the low-velocity flow-conditions presented.

For a slightly soluble compound, such as BA, the dissolution would have a minor effect on local hydrodynamics. The effects of flow-reversal due to the adverse pressure gradient during the deceleration phase of pulse inflow was the main factor affecting local hydrodynamics, causing a lower flow near the surface and consequently lower dissolution rate than the free convection system. A simulation, therefore, of hydrodynamics alone would be informative in interpreting dissolution rates of a slightly soluble compound in this low velocity pulsing flow.

An estimate of boundary layer thickness from a simulation using species transfer should be able to predict the influence of the hydrodynamic environment, accounting for both forced and natural convection, on dissolution rate. The variation in predicted boundary layer thickness at different locations and at different time points suggest possible non-uniform dissolution in low-velocity flow fields in the flow-through apparatus. The results indicate that the dissolution rate during a short time frame at locations near the dissolving surface may be more complex than regular effluent measurements would suggest. This is of relevance for situations where a dissolving surface may encounter non-sink conditions, for example during certain phases of its journey through the gastro-intestinal tract, where it may encounter low fluid volumes (Schiller et al., 2005). Furthermore, the results suggest that a freely soluble excipient, such as LM, may affect the

local hydrodynamic environment during dissolution testing of a low solubility active ingredient. As low fluid velocity environments have been used in order to create more biorelevant agitation conditions, the effect of natural convection on the local hydrodynamic environment, and therefore the dissolution rate, is a factor which needs to be considered when attempting to generate biorelevant dissolution data. This may have particular relevance in early formulation development when excipients of different solubilities may be used, thereby having different effects on local hydrodynamics via natural convection.

Acknowledgement:

The authors gratefully acknowledge the post-graduate research scholarship for Bo Liu from the Irish Research Council for Science Engineering and Technology (IRCSET), which has funded this research.

References

Bhattachar, S. S., J. A. Wesley, et al., 2002. Dissolution testing of a poorly soluble compound using the flow-through cell dissolution apparatus. Int J Pharm **236**: 135-143.

Butler, W. and S. Bateman, 1998. A flow-through dissolution method for a two component drug formulation where the actives have markedly differing solubility properties Int J Pharm **173**(1-2): 211-219.

Cammarn, S. R. and A. Sakr, 2000. Predicting dissolution via hydrodynamics: salicylic acid tablets in flow through cell dissolution. Int J Pharm **201**: 199-209.

Cammarn , S. R. and A. Sakr, 2000. Predicting dissolution via hydrodynamics: salicylic acid tablets in flow through cell dissolution. Int J Pharm **201**: 199-209.

600 D'Arcy, D. M., O. I. Corrigan, et al., 2005. Hydrodynamic simulation(computational fluid dynamics) of asymmetrically positioned tablets in the paddle dissolution apparatus: impact on dissolution rate and variability. Journal of Pharmacy and Pharmacology **57**: 1-9.

D'Arcy, D. M., A. M. Healy, et al., 2009. Towards determining appropriate hydrodynamic conditions for in vitro in vivo correlations using computational fulid dynamics. European
605 Journal of Pharmaceutical Sciences **37**(3-4): 291-299.

D'Arcy, D. M., B. Liu, et al., 2010. Hydrodynamic and species transfer simulations in the USP 4 dissolution apparatus: considerations for dissolution in a low velocity pulsing flow. Pharmaceutical Research **27**(2): 246-258.

D'Arcy, D. M. and T. Persoons, 2011. Mechanistic modelling and mechanistic mointoring:
610 simulation and shadowgraph imaging of particulate dissolution in the flow-through apparatus. Journal of Pharmaceutical Sciences **DOI 10.1002/jps**.

Diebold, S., 2005. Physiological parameters relevant to dissolution testing: hydrodynamic considerations. Pharmaceutical Dissolution Testing. J. Dressman and J. Krämer. Boca Raton, Taylor and Francis Group.

615 Dokoumetzidis, A., V. Papadopoulou, et al., 2008. Development of a reaction-limited model of dissolution: Application to official dissolution tests experiments Int J Pharm **355**(1-2): 114-125.

Edwards, L. J., 1951. The dissolution and diffusion of aspirin in aqueous media. Trans. Faraday Soc. **47**: 19.

620 Fang, J., V. Robertson, et al., 2010. Development and Applicantion of a Biorelevant Dissolution Method Using USP Apparatus 4 in Early Phase Formulation Development. Molecular Pharmaceutics.

Fluent(Inc.) (2003). Fluent User's Guide. Fluent Documentation 6.1. Lebanon, NH, USA, Fluent (Ansys) Inc.

Fotaki, N. and C. Reppas, 2005. The flow through cell methodology in the evaluation of intralumenal drug release characteristics. Dissolution Technologies **12**(2): 17-21.

Goldberg, A. H. and W. I. Higuchi, 1968. Improved method for diffusion coefficient determinations employing the silver membrane filter. Journal of Pharmaceutical Sciences **57**(9): 1583-1585.

Graffner, C., M. Särkelä, et al., 1996. Use of statistical experimental design in the further development of a discriminating in vitro release test for ethyl cellulose ER-coated spheres of remoxipride. Eur J Pharm Sci **4**: 73-83.

JP, 2006. Japanese Pharmacopoeia. Japan, Ministry of Health, Labour and Welfare.

Kakhi, M., 2009a. Classification of the flow regimes in the flow-through cell European Journal of Pharmaceutical Sciences **37**(5): 531-544.

Kakhi, M., 2009b. Mathematical modeling of the fluid dynamics in the flownext term-through cell International Journal of Pharmaceutics **376**(1-2): 22-40.

Pal, A., K. Indireshkumar, et al., 2004. Gastric flow and mixing studied using computer simulation. Proc. R. Soc. Lond., B, Biol. Sci. **271**: 2587-2594.

Ph.Eur., 2011. European Pharmacopoeia. Strasbourg, France, European Directorate for the Quality of Medicines and HealthCare (EDQM), Council of Europe.

Phillips, J., Y. Chen, et al., 1989. A flow-through dissolution approach to in vivo/in vitro correlation of adinazolam release from sustained release formulations. Drug Dev Ind Pharm **15**: 2177-2195.

Ramtoola, Z. and O. I. Corrigan, 1987. Dissolution Characteristics of Benzoic Acid and Salicylic Acid Mixture in Reactive Media. Drug Development and Industrial pharmacy **13**: 1703-1720.

Schiller, C., C.-P. Frölich, et al., 2005. Intestinal fluid volumes and transit of dosage forms as assessed by magnetic resonance imaging. Aliment. Pharmacol. Ther. **22**: 971-919.

Shiko, G., L. F. Gladden, et al., 2010. MRI studies of the hydrodynamics in a USP 4 dissolution testing cell. Journal of Pharmaceutical Sciences **DOI 10.1002/jps**.

Stevens , L. E. and P. J. Missel, 2006. Impact of density gradients on flow-through dissolution in a cylindrical flow cell. Pharm Dev Technol **11**: 529-534.

Sunesen, V., B. Pedersen, et al., 2005. In vivo in vitro correlations for a poorly soluble drug, danazol, using the flow through dissolution metthod with biorelevant dissolution media. Eur J Pharm Sci **24**: 305-313.

Sunesen, V. H., B. L. Pedersen, et al., 2005. In vivo in vitro correlations for a poorly soluble drug, danazol, using the flow-through dissolution method with biorelevant dissolution media. Eur J Pharm Sci **24**: 305-313.

USP, 2011. United States Pharmacopeia 34-National Formulary 29. Rockwell, MD, USA.

Venancio, A. and J. A. Teixeira, 1997. Characerization of sugar diffusion coefficients in alginate membranes. Biotechnology Techniques **11**(3): 183-186.

Weitschies, W., H. Blume, et al., 2010. Magnetic marker monitoring: high resolution real-time tracking of oral solid dosage forms in the gastrointestinal tract. Eur J Pharm Biopharm **74**: 93-101.

Wu, Y. and E. S. Ghaly, 2006. Effect of hydrodynamic environment on tablet dissolution using flow-through dissolution apparatus. Puerto Rico Health Sciences Journal **25**(1): 75-83.

Zhang, G. H., W. A. Vadino, et al., 1994. Evaluation of the flow-through cell dissolution apparatus: effects of flow rate, glass beads and tablet position on drug release from different type of tablets. Drug Dev Ind Pharm **20**(13): 2063-2078.

Figure Captions

Figure 1. *The flow-through apparatus and free convection system models.* Diagram illustrating A) the 2D model of the flow-through apparatus and B) the 2D model of the free convection system. The horizontal lines used in the simulations to determine local velocity values in the flow-through apparatus (lines A-E) and the free convection system (lines A-C) are also illustrated. The dissolving surface is the left vertical planar surface.

Figure 2. *Velocity vectors from the BA species transfer flow-through apparatus simulation.* Vectors colored by velocity magnitude (m s^{-1}) from the BA species transfer simulation in the flow-through apparatus at A) 0.03s; B) 0.13s; C) 0.23s; D) 4.03s; E) 4.13s and F) 4.23s. A-C are defined as the initial state and D-F are from steady state simulations.

Figure 3. *Velocities in the flow-through apparatus BA species transfer simulation.* Data from horizontal lines A-E in the flow-through apparatus from the simulation using BA species transfer, showing velocity magnitude (m s^{-1}) vs. distance from compact surface at the point of maximum inflow (0.13s timepoint of pulse). A) initial state, 0.13s, B) steady state, 4.13s.

Figure 4. *Velocity vectors in the free convection system.* Vectors colored by velocity magnitude (m s^{-1}) from the A) BA species transfer simulation and B) the LM species transfer simulation of hydrodynamics in the free convection system, at steady state. 1 vector in 190 shown for clarity.

Figure 5. *Estimates of diffusion boundary layer thickness.* Estimated boundary layer thickness along the central horizontal line at different time points of the pulse, from species transfer simulations in the flow-through apparatus (BA ♦, LM ▲) and free convection system (BA ■, LM x).

Figure 6. *Velocity vectors from the LM species transfer flow-through apparatus simulation* .Vectors colored by velocity magnitude (m s^{-1}) from the LM species transfer

simulation in the flow-through apparatus at A) 0.03s; B) 0.13s; C) 0.23s; D) 6.03s; E) 6.13s and F) 6.23s. A-C are defined as the initial state and D-F are from steady state simulations

Figure 7. *Velocities in the flow-through apparatus LM species transfer simulation.* Data from horizontal lines A-E in the flow-through apparatus from the simulation using LM species transfer, showing velocity magnitude (m s^{-1}) vs. distance from compact surface at the point of maximum inflow (0.13s time point of pulse) at steady state.

Table 1: The dissolution rate of BA and LM (mg min^{-1} cm^{-2}), in the different dissolution apparatuses and the effective diffusion boundary layer thickness, h (equation 1).

BA	***G* (mg min^{-1} cm^{-2}) +/- SD**	**h (m x 10^6)**
Free convection system	0.123 +/- 0.003 [1]	275
Flow-through apparatus (USP 4)	0.094 +/- 0.008 [1]	360
Paddle apparatus (USP 2)	0.441+/-0.036	76
LM	***G* (mg min^{-1} cm^{-2}) +/- SD**	**h (m x 10^6)**
Free convection system	6.89 +/- 1.70	61
Flow-through apparatus	3.24 +/- 0.69	130
Paddle apparatus	8.52 +/- 0.399	49

1. Dissolution rates for BA in the flow-through apparatus and free convection system are taken from D'Arcy, et al., 2010

Figure 1

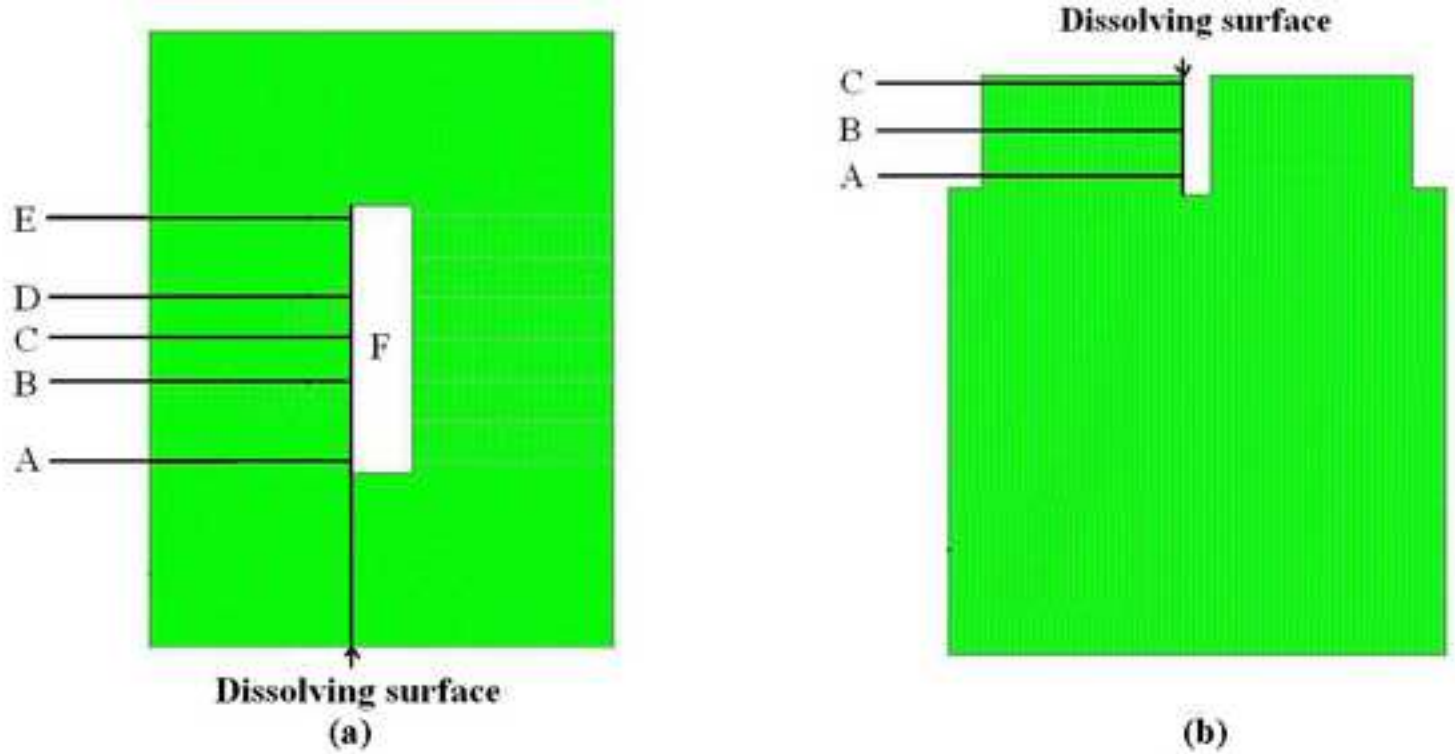

Figure 2

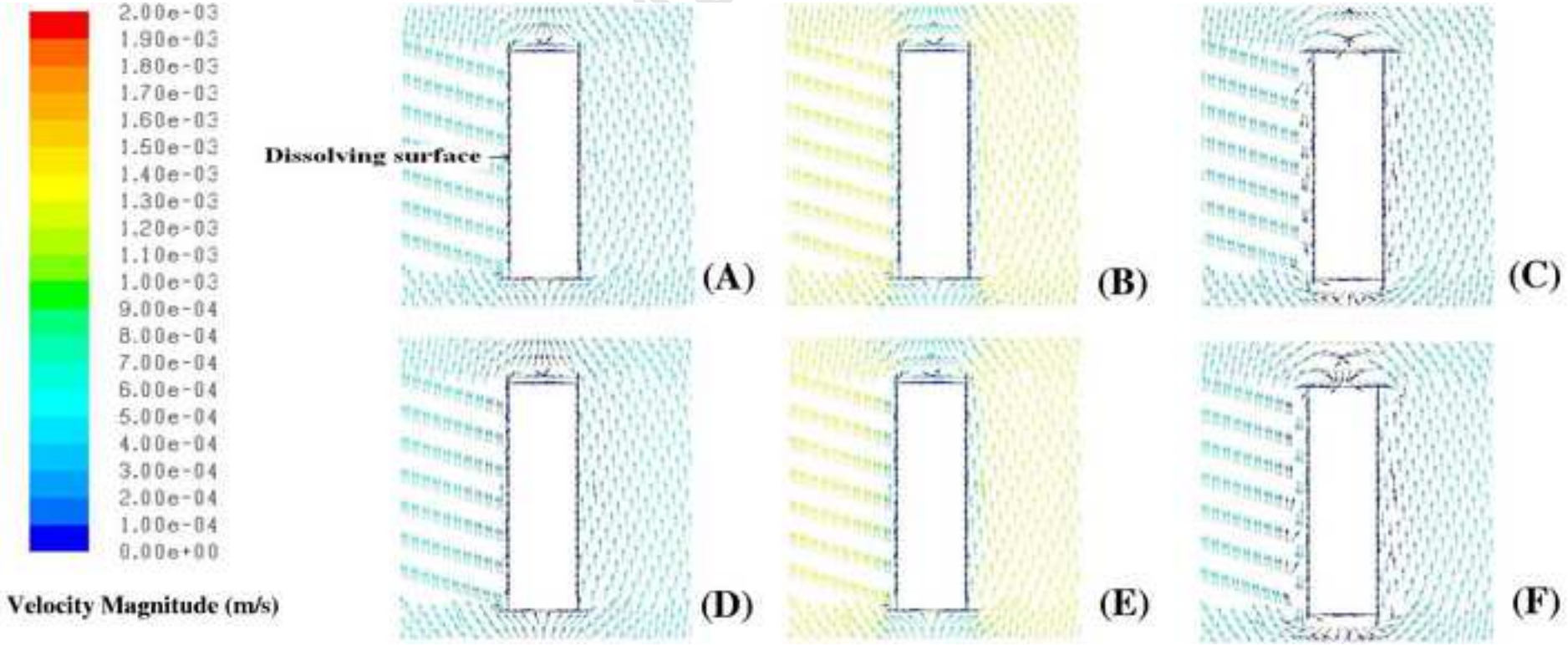
2.00e-03
1.90e-03
1.80e-03
1.70e-03
1.60e-03
1.50e-03
1.40e-03
1.30e-03
1.20e-03
1.10e-03
1.00e-03
9.00e-04
8.00e-04
7.00e-04
6.00e-04
5.00e-04
4.00e-04
3.00e-04
2.00e-04
1.00e-04
0.00e+00
Velocity Magnitude (m/s)
Dissolving surface
(A)
(B)
(C)
(D)
(E)
(F)

Figure 3

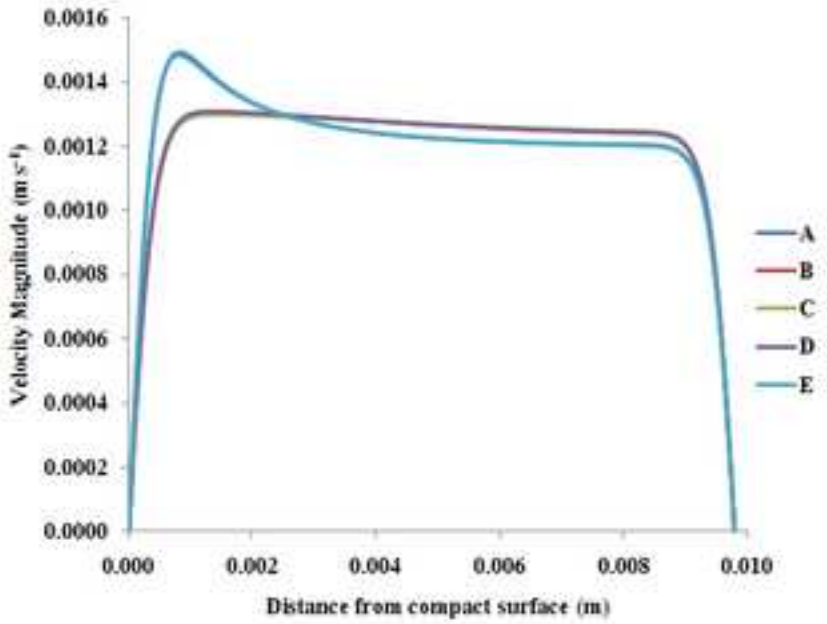
0.0016
0.0014
0.0012
0.0010
0.0008
0.0006
0.0004
0.0002
0.0000
Velocity Magnitude (m s⁻¹)
0.000
0.002
0.004
0.006
0.008
0.010
Distance from compact surface (m)
A
B
C
D
E

(A)

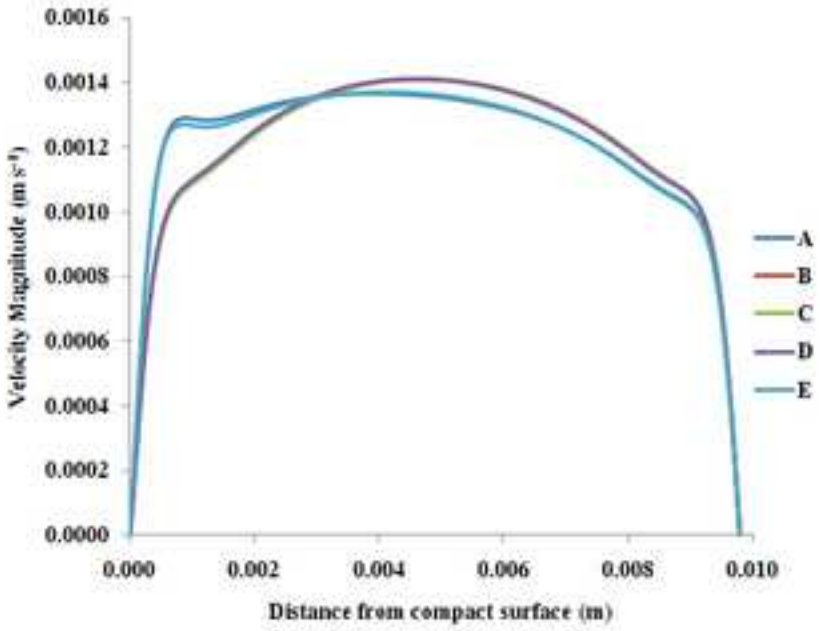
0.0016
0.0014
0.0012
0.0010
0.0008
0.0006
0.0004
0.0002
0.0000
Velocity Magnitude (m s⁻¹)
0.000
0.002
0.004
0.006
0.008
0.010
Distance from compact surface (m)
A
B
C
D
E

(B)

Figure 4

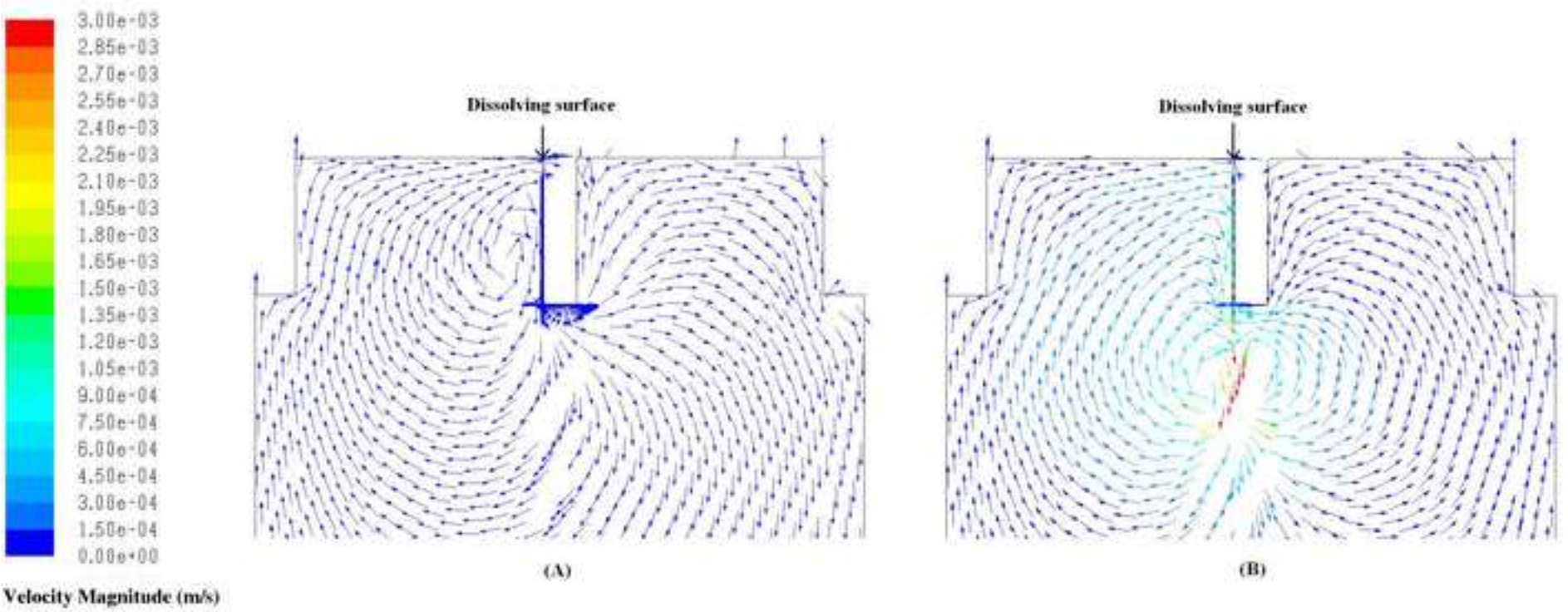
3.00e-03
2.85e-03
2.70e-03
2.55e-03
2.40e-03
2.25e-03
2.10e-03
1.95e-03
1.80e-03
1.65e-03
1.50e-03
1.35e-03
1.20e-03
1.05e-03
9.00e-04
7.50e-04
6.00e-04
4.50e-04
3.00e-04
1.50e-04
0.00e+00
Velocity Magnitude (m/s)
Dissolving surface
(A)
Dissolving surface
(B)

Figure 5

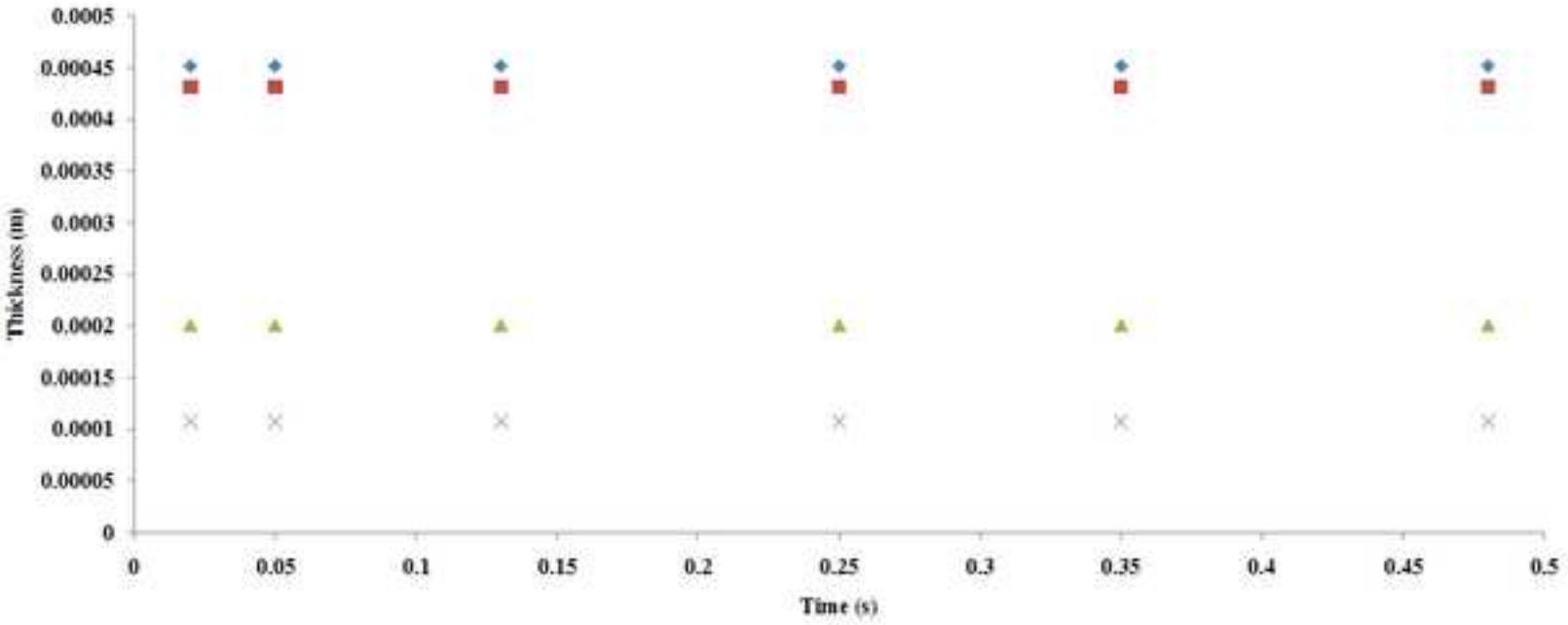
0.0005
0.00045
0.0004
0.00035
0.0003
0.00025
0.0002
0.00015
0.0001
0.00005
0
Thickness (m)
0
0.05
0.1
0.15
0.2
0.25
0.3
0.35
0.4
0.45
0.5
Time (s)

Figure 6

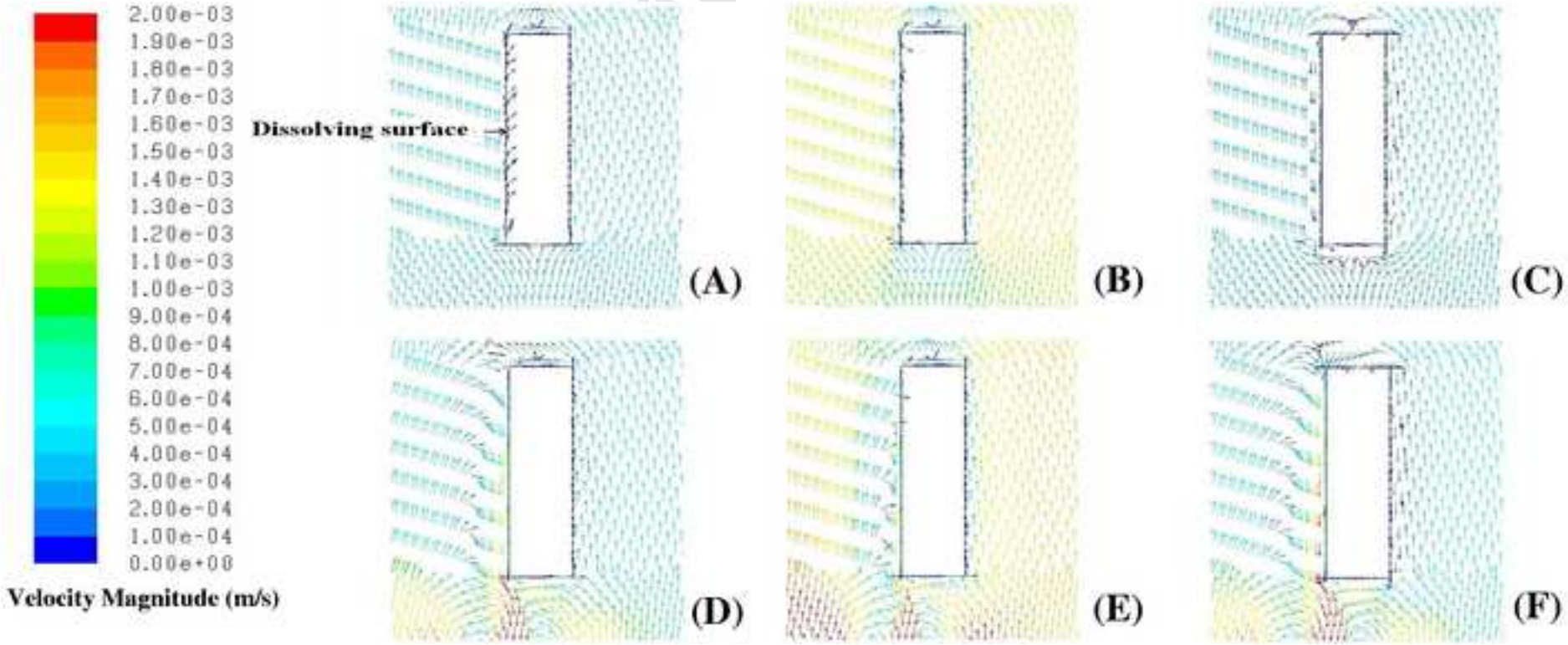
2.00e-03
1.90e-03
1.80e-03
1.70e-03
1.60e-03
1.50e-03
1.40e-03
1.30e-03
1.20e-03
1.10e-03
1.00e-03
9.00e-04
8.00e-04
7.00e-04
6.00e-04
5.00e-04
4.00e-04
3.00e-04
2.00e-04
1.00e-04
0.00e+00
Velocity Magnitude (m/s)
Dissolving surface
(A)
(B)
(C)
(D)
(E)
(F)

Figure 7

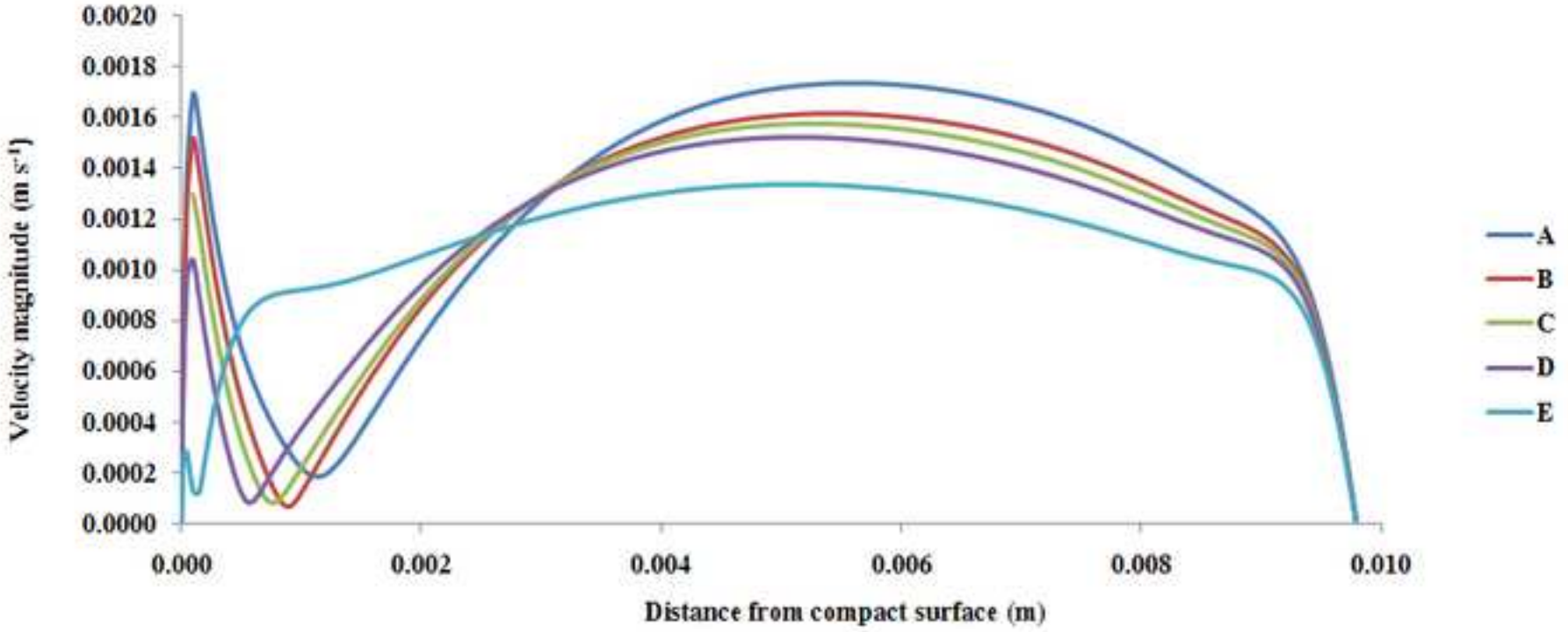
Velocity magnitude (m s-1)
0.0020
0.0018
0.0016
0.0014
0.0012
0.0010
0.0008
0.0006
0.0004
0.0002
0.0000
0.000
0.002
0.004
0.006
0.008
0.010
Distance from compact surface (m)
A
B
C
D
E